Al-MFI Nanosheets as Highly Active and Stable Catalysts for the Conversion of Propanal to Hydrocarbons

Citation: Luo, Helen, Teerawit Prasomsri, and Yuriy Román-Leshkov. "Al-MFI Nanosheets as Highly Active and Stable Catalysts for the Conversion of Propanal to Hydrocarbons." Top Catal 58, no. 7–9 (March 31, 2015): 529–536.

As Published: http://dx.doi.org/10.1007/s11244-015-0394-9

Publisher: Springer US

Persistent URL: http://hdl.handle.net/1721.1/103357

Version: Author's final manuscript: final author's manuscript post peer review, without publisher's formatting or copy editing

Al-MFI nanosheets as highly active and stable catalysts for the conversion of propanal to hydrocarbons

Helen Luo, Teerawit Prasomsri, Yuriy Román-Leshkov*

Department of Chemical Engineering, Massachusetts Institute of Technology, Cambridge, MA 02139

*Corresponding Author: yroman@mit.edu; Phone: (+1) 617-253-7090

Abstract

The conversion of propanal to hydrocarbons was investigated over mesoporous aluminosilicate MFI nanosheets (Al-MFI-ns) of single-unit-cell thickness and conventional aluminum MFI zeolite (Al-MFI) at 673 K and atmospheric pressure. Al-MFI-ns exhibited a five-fold increase in stability attributed to the shorter diffusion path lengths and open architecture of the nanosheets, which minimized pore blocking from fouling. The overall ratio of olefin to aromatic products was similar for Al-MFI-ns and Al-MFI at all conversion levels. However, the product distribution within each group shows that the Al-MFI-ns features a five-fold increase in selectivity to C_{6-8} olefins and a two-fold increase in selectivity to C_{9-10} aromatics compared to Al-MFI. The very high selectivity to C_9 aromatic trimethylbenzene supports an aromatization mechanism involving sequential aldol condensation and dehydration sequences. The very short diffusion paths from the single-unit-cell thick nanosheets allows for the C_9 aromatics to diffuse out of the pores before they can be converted to lighter aromatics or olefins by way of a regular hydrocarbon pool mechanism. Al-MFI-ns shows no indication of irreversible deactivation, fully recovering its original activity after regeneration by calcination, and retaining similar deactivation rates and product selectivities as the fresh catalyst. Al-FMI-ns improves results for production of aromatics from light oxygenates at mild conditions, a key reaction for bio-oil upgrading.

Keywords: bio-oil upgrading, propanal to hydrocarbons, hierarchical zeolites, aromatization, nanosheets

Dedication

This article is dedicated to Prof. Mark E. Davis, a great mentor and friend, who recently received the prestigious Somorjai award honouring his important contributions to the field of molecular sieves. Undoubtedly, his work has shaped our understanding of solid acid chemistry and catalysis with porous materials. While his work has profoundly impacted many research areas in both industrial and academic settings, an equally important aspect of his contributions have stemmed from mentoring and inspiring those around him to take risks and undertake new, challenging research directions. During my postdoctoral stay in his group from 2008-2010, we explored the use of solid Lewis acids, such as Sn-Beta, for the activation carbohydrates.[1-3] In turn, this work strongly influenced the research direction undertaken in my independent academic career, including, for example, the use of hafnium-based materials to activate oxygenates.[4, 5] In this contribution, we show how controlling the morphology of zeolite crystals through amphiphilic structure directing agents that produce nanosheets results in materials with drastically higher stability and lifetime for the conversion of short oxygenates to aromatics.

1 Introduction

Fast pyrolysis bio-oil contains a large fraction of small oxygenates (< C_6), which are thermally and chemically unstable [6]. These oxygenate species containing aldehyde, alcohol, and acid functional groups lower the heating value, increase the vapor pressure, and may further oxidize and polymerize other components to create corrosive and heavy products during storage and transportation. Upgrading by deoxygenation is required to convert these compounds to fuel-compatible molecules. While hydrotreating allows us to convert light oxygenates to gases at high temperatures and H_2 pressures, a more attractive approach is to upgrade these oxygenates via hydrodeoxygenation at mild conditions [7, 8] followed by alkylation or by condensation and aromatization to larger and more stable hydrocarbon molecules [9, 10].

Aluminosilicate zeolite catalysts such as H-ZSM-5 have been extensively studied for bio-oil upgrading as well as the conversion of methanol to hydrocarbons [11-14]. Zeolites can catalyze shape-selective reactions due to their high density of strong Brønsted acid sites and their uniform microporous channel system. However, microporosity can hinder diffusion of bulky molecules resulting in decreased apparent rates and faster deactivation by fouling from coke deposition [15]. Hierarchical zeolites that contain both mesoporous and microporous pores can improve the traffic of reactants and products by shortening intracrystalline diffusion lengths. Importantly, hierarchical zeolites are fully crystalline, unlike conventional mesoporous materials such as MCM-41, thereby displaying high hydrothermal stability and strong Brønsted acidity [16].

Hierarchical zeolites have been obtained by desilication [17, 18] or dealumination [19], delamination [20, 21], pillaring [22], and confined growth in hard templates [23]. Recently, Ryoo and co-workers developed a one-step synthetic method to make zeolite nanosheets with single-unit-cell thickness [24]. Upon calcination, these nanosheets would collapse in a disorderly manner forming highly connected intersheet mesopores. The synthesis uses a surfactant-like organic structure-direction-agent (SDA), which consists of a hydrophilic diquaternary ammonium head and a paraffinic hydrophobic tail. The head directs the formation of the zeolite micropores, while the tail prevents growth in one spatial dimension. Aluminum-containing zeolite nanosheets of MFI topology (Al-MFI-ns) show high catalytic activity in a variety of acid-catalyzed reactions such as Friedel-Crafts alkylations [25], methanol-to-olefins [26], and methanol-to-hydrocarbons [24].

Here, we report on the catalytic activity, and stability of Al-MFI-ns for the conversion of small oxygenates to hydrocarbons. Specifically, we study the model reaction of propanal (a surrogate model compound representing aldehydes in bio-oil) to hydrocarbons, which suffers from very rapid catalyst deactivation from coke deposition [27-29]. We find that the Al-MFI-ns are more stable than bulk H-ZSM-5 (Al-MFI), and deactivate at a much slower rate at comparable space velocities. Although a similar product distribution for both catalysts in terms of total olefin and aromatics production is observed, the more open structure of Al-MFI-ns results in higher yields of larger (C_9 and C_{10}) aromatics. We find that original catalyst activity can be fully recovered after calcination, while retaining the same product distributions after two regeneration cycles in a flow reactor. Designing heterogeneous catalysts that are more stable to deactivation is crucial for developing industrially viable processes, particularly for the upgrading of biomass-derived feedstock.

2 Experimental

2.1 Catalyst synthesis and characterization

Specific details of the synthesis and characterization of Al-MFI-ns used in this study can be found in our previous work [30]. Al-MFI-ns material was synthesized following the procedures developed by Choi *et al*. [24]. Briefly, $[C_{22}H_{33}\text{-}N^{+}(CH_3)_2\text{-}C_6H_{12}\text{-}N^{+}(CH_3)_2\text{-}C_6H_{13}][OH^{-}]_2$ designated as $C_{22\text{-}6\text{-}6}$ was synthesized through two consecutive S_N2 reactions in acetonitrile with intermediate purification by filtering, and an ion-exchange from bromide to hydroxide form. Using this SDA, Al-MFI-ns were prepared by mixing tetraethylorthosilicate (Sigma-Aldrich, 99% (w/w)), pseudoboehmite (Sasol, Catapal B 70% (w/w) Al_2O_3), and aqueous $C_{22\text{-}6\text{-}6}$ were added to a PTFE dish and aged at 333 K for 6 h. The final molar composition of the synthesis gel was 0.02 Al_2O_3 / 1 SiO_2 / 0.13 SDA / 60 H_2O. The solution was transferred to a PTFE-lined stainless steel autoclave and heated at 423 K for 9 days. The solids were recovered by filtration, extensively washed with deionized water, dried at 373 K overnight and calcined at 823 K for 10 h. Al-MFI was purchased from Zeolyst International with ID number CBV 3024E.

Catalysts were characterized with powder X-ray diffraction (PXRD) collected on a Bruker D8 diffractometer using Cu Kα radiation (40 kV, 40 mA). Surface area and pore volumes were determined from N_2 adsorption isotherms measured on a Quantachrome Autosorb iQ apparatus at 77 K. Prior to analysis, all samples were degassed under vacuum for 12 h at 623 K. SEM images were taken at a low electron acceleration voltage with an SEI detector (JEOL 6700F, 3mm WD, 1 kV) without a metal coating, after mounting the samples on a carbon-coated tape. TEM images were obtained using a JEOL 2010 at an operating voltage of 200 kV. Elemental analysis was performed by dissolving samples in 48% (w/w) HF, diluting into 3% HNO_3, and measuring concentration on a CCD-based inductively coupled plasma (ICP) atomic emission spectrometer (Activa-S, HORIBA Scientific). A 5-point calibration curve was built using a 1000 ppm Al standard in 2% HNO_3 (TraceCERT) on the 167.020 nm Al spectral line. ^{27}Al solid-state MAS NMR spectra were recorded using a Bruker DSX 500 spectrometer operating at 11.7 T with 130.3 MHz for 27Al nuclei, using a Bruker 4 mm CPMAS probe. Spinning rates of 15 kHz were used and MAS spectra were recorded after applying a 0.3 μs-π/18 pulse for the 27Al nucleus. Peak deconvolution was performed in OriginLab using Lorentz function fitting.

Simulated XRD patterns were generated using powder pattern theorem implemented with UDSKIP [31, 32]. Atomic coordinates for zeolite MFI structure were obtained from Koningsveld *et al* [33]. The simulated crystal had dimensions of 10 unit cells in the *a* and *c* direction, and 1 unit cell in the *b* direction. Simulations for the wide-angle X-ray diffraction were carried out with a step size $2\theta = 0.02^{o}$ (Cu Kα radiation).

2.2 Propanal to hydrocarbons catalytic studies

Catalytic testing experiments were conducted in a vapor-phase packed-bed flow reactor system. A stainless steel tube reactor ¼" OD was mounted in an insulated single-zone furnace (850W/ 115V, Applied Test Systems Series 3210). Temperature was controlled at 673 K using a thermocouple mounted in the catalyst bed (Omega, model TJ36-CAXL-116u) connected to a temperature controller (Digi-Sense, model 68900-10). The zeolite catalyst bed (40-200 mg) was mixed with an inert (α-alumina, Sigma Aldrich) and sieved to a size of 75-150 μm to reach a final bed volume of 2 ml. Propanal (Sigma Aldrich, 97% (w/w)) was introduced into the reactor via a syringe pump (Harvard Apparatus, model 703005) at a rate of 0.2 ml h^{-1}. The reaction was carried out at atmospheric pressure at different space velocities (SV), defined as the ratio of mole feed rate to mole Brønsted acid sites in the catalyst, ranging from 50 to 100 h^{-1}, with a He carrier gas flow rate of 70 ml min^{-1}. Catalyst was regenerated by calcining *in situ* at 873 K under dry air flow for 1 h.

The reactor effluent lines were heated at 523 K to prevent condensation of products, which were directly analyzed and quantified by an online gas chromotographer (GC) equipped with a flame ionization detector (7890A GC-FID, Agilent Technologies) and a HP-1 column (Agilent, 30 m × 0.25 mm id, 0.25 μm). The GC was operating with ultra-high purity He as a carrier gas at a constant flow rate of 1.0 ml min^{-1}. Products were identified using a mass selective detector (5975C MSD, Agilent Technologies). Conversion is defined as: mole of carbon reacted / mole of carbon in the feed. Yield of product group *i* is defined as: mole of carbon produced as compounds in product group *i* / mole of carbon in the feed. Selectivity of product *j* is defined as: mole of carbon produced as product *j* / mole of carbon produced as compounds in the product group that includes product *j*.

3 Results and Discussion

3.1 Characterization of Al-MFI catalysts

Characterization data for Al-containing zeolite catalysts are shown in Figure 1 and Table 1. PXRD spectra confirm the presence of the MFI topology for both Al-MFI and Al-MFI-ns; however, the diffraction pattern for Al-MFI-ns features broader peaks and contains reflections primarily belonging to (*h0l*) lattice planes. Simulated diffraction patterns obtained using UDSKIP, for MFI crystal fragments that are 10 unit cells wide along the *a*- and *c*-axes and one unit cell thick along the *b*-axis, are in good agreement with the experimental Al-MFI-ns PXRD pattern (see Figure 1A). The Al-MFI-ns patterns show considerable peak-broadening and a dramatic decrease in peak intensity for reflections associated with long-range order along the *b*-axis. SEM and TEM were used to explore the structure and morphology of the nanosheets. SEM images of Al-MFI-ns reveal large agglomerations, 1-1.5μm in size, composed of disordered platelets (Figure 1B). No other morphologies were detected during low-magnification inspections indicating a pure MFI nanosheet phase material. TEM imaging confirmed the presence of lamellae ~2 nm thick along the (101) direction and 50-100 nm wide along the (100) and (001) directions (Figure 1C). The morphology of Al-MFI features much larger crystals ca. 300 nm in diameter.

Elemental analysis reveals the aluminum content of Al-MFI-ns is 1.7%, which corresponds to an effective Si/Al = 26. This value is very close to the theoretical value of Si/Al = 25 used in the synthesis gel. Nitrogen adsorption isotherms revealed that the micropore volume of Al-MFI-ns is 0.142 cm^3g^{-1}, slightly smaller than that of Al-MFI at 0.158 cm^3g^{-1}. However, the external surface area of Al-MFI-ns after calcination is 357 m^2g^{-1}, which is much larger than the external surface area of Al-MFI (likely < 80 m^2g^{-1} based on crystal size) due to the formation of disordered mesopores. This increase in mesoporosity is reflected in a much larger total pore volume for Al-MFI-ns (0.552 cm^3g^{-1}) than that of Al-MFI (0.255 cm^3g^{-1}).

Brønsted acid sites were characterized and quantified by probing the Al coordination using ^{27}Al solid state magic angle spinning nuclear magnetic resonance (MAS NMR). Octahedral, pentahedral, and tetrahedral Al have chemical shifts located at 0, 25, and 50 ppm respectively. Octahedrally and pentahedrally coordinated sites indicate extraframework Al, which may exhibit Lewis acid behavior. Tetrahedrally coordinated sites indicate framework Al, which exhibits Brønsted acid behavior when the zeolite is in the proton form. Quantification of the NMR data

revealed that the Al-MFI-ns contained a significant amount of extraframework Al, possibly due to incomplete dissolution of the aluminum precursor, pseudoboehmite, during synthesis. Although significant, this extraframework Al is not active for conversion of propanal to hydrocarbons. In contrast to the 43.8% tetrahedral Al sites in Al-MFI-ns, Al-MFI had 86.2% tetrahedral Al sites. The differences in total aluminum content and number of tetrahedral Brønsted acid sites between the two catalysts results in Al-MFI having 3.3 times more Brønsted acid sites per gram catalyst than Al-MFI-ns.

3.2 Catalyst stability and product selectivity

Propanal conversion was investigated over Al-MFI-ns and Al-MFI at 673 K and atmospheric pressure. Al-MFI starts to rapidly deactivate after 1.5 h time-on-stream (TOS) resulting in a 70% drop in activity after only 3 h TOS at SV = 75 h^{-1} (Figure 2). In contrast, Al-MFI-ns deactivates at a much slower rate with only a 15% drop in activity after 3 h TOS even at a higher SV = 100 h^{-1}. Lowering the space velocity by half to SV = 50 h^{-1} halves the deactivation rate from ~5% per hour to ~2.5% per hour. This behavior agrees well with what we would expect to see if the primary mechanism for deactivation was from fouling due to coke deposition. Al-MFI has much longer diffusion paths than the single-unit-cell thick Al-MFI-ns. Since longer diffusion paths allow more time for products to form coke precursors and coke, Al-MFI suffers from much faster deactivation. In addition the open structure of Al-MFI-ns would decrease the effects of fouling, since there are a larger fraction of accessible micropore openings within the mesopores.

To simplify our comparison, the products are divided into three main groups: incondensable gases (C_{1-2}, primarily CO_2), olefins (C_{3-8}, primarily propylene), and aromatics (C_{6-10}, primarily toluene and xylenes). Figure 3 combines the SV and TOS data and shows that very similar trends were observed for product yields as a function of conversion for both Al-MFI-ns and Al-MFI. The yield of incondensable gases, including methane, CO_2, and CO, remained <10% throughout the entire range of conversions. The aromatics yields increase rapidly with increasing conversion from 5% aromatics yield at 30% conversion to 60% aromatics yield at 100% conversion, overtaking the olefin yield at 80% conversion for both catalysts. The olefins yield increases slightly with increasing conversion from ~25% to a maximum of 40% at 80% conversion. The similarity in the ratio of olefins to aromatics between both catalysts at all conversions indicates that the local environment of the Brønsted acid sites is not significantly

changed with crystal morphology. In addition, the space velocity and TOS data for each catalyst falls on the same line implying that the deactivation that occurs at longer TOS only results in a reduction in the number of active sites.

The product selectivity within the olefin and aromatics groups changes significantly between Al-MFI-ns and Al-MFI. As expected, the more open mesoporous structure of Al-MFI-ns generates a higher selectivity toward C_6-C_8 olefins and C_9-C_{10} aromatics (Figure 4). At conversion levels close to 100%, Al-MFI-ns generate a C_6-C_8 olefin selectivity of ~25%, whereas Al-MFI generates a C_6-C_8 olefin selectivity of ~5%. Similarly, for the aromatic products, Al-MFI-ns features a C_9-C_{10} aromatics selectivity of ~60%, while Al-MFI features a C_9-C_{10} aromatics selectivity of ~30% at similar conversion levels. The MFI-topology consists of 10 member ring pores that form a 3-dimensional channel system with window openings of 0.54×0.56 nm and 0.51×0.55 nm and channel intersections with a maximum diameter of 0.9 nm. Aromatic molecules such as benzene, which has a critical diameter of 0.68 nm, can form within pore intersections and diffuse out, however the narrow channels will reduce their effective diffusion constants [34]. These differences in diffusion rates between the different sized products can modify the selectivity. Since the Al-MFI-ns are only one unit cell wide (~2 nm), the drastic shortening of intracrystalline diffusion paths leads to significant increases in larger olefins and aromatics production.

A very interesting observation is the very high selectivity ~60% to C_9 trimethylbenzene at conversions from 40-100% over Al-MFI-ns (Figure 4D). It is generally accepted that aromatization of small molecules over zeolite acid catalysts occurs via oligomerization of intermediate olefins forming a hydrocarbon pool, which generates aromatics and olefins [13]. Recently, Hoang *et al*. proposed an alternate reaction pathway where C_9 aromatics can be produced by cyclization and dehydration of aldol trimers formed from propanal via aldol self-condensations [35]. These C_9 aromatics can then be cracked into smaller secondary aromatic products or coke if they remain within the zeolite channels. Since the diffusion path length of Al-MFI-ns is very short, the C_9 aromatics formed from this alternate mechanism leave the channels before further cracking, resulting in their high selectivity. Alternatively, these C_9 compounds can also be formed directly on the large fraction of external acid sites in Al-MFI-ns. Increasing the selectivity to larger fuel-compatible compounds of oxygenates to hydrocarbons allows us to obtain a higher liquid yield.

3.3 Catalyst regeneration

After 5 h TOS, the Al-MFI-ns was calcined *in situ* under flowing air at 873 K for 1 h. As shown in Figure 5, the original catalyst activity was fully recovered, and the regenerated catalyst showed a similar deactivation behavior as that of the fresh catalyst. Specifically, there was no change in the product distributions when using regenerated catalyst. After two regeneration cycles, the relative amounts of olefins and aromatics remains the same as a function of conversion, crossing over at ~80% conversion. Al-MFI-ns are stable after two regeneration cycles, showing no indication of irreversible deactivation after 16 h TOS corresponding to a total TON of 1410 mole propanal per mole Brønsted acid sites.

4 Conclusions

Al-MFI-ns are active and stable catalysts for the conversion of propanal to hydrocarbons, featuring deactivation rates that are nearly five times slower than the conventional Al-MFI catalyst at similar space velocities. The open mesoporous structure of the Al-MFI-ns results in a drastic shortening of reactant and product diffusion path lengths as well as an increased number of pore openings, reducing the effects of fouling allowing for a longer catalyst lifetime. The ratio of total olefin products to total aromatic products as a function of conversion are very similar for both Al-MFI-ns and Al-MFI, and are independent of TOS, implying that deactivation mainly reduces the number of active sites rather than changing their intrinsic activity. However, the product distribution within each group shows that the Al-MFI-ns give a five-fold increase in selectivity to C_{6-8} olefins and a two-fold increase in selectivity to C_{9-10} aromatics compared to Al-MFI. The very high selectivity to C_9 aromatic trimethylbenzene supports an alternative aromatization mechanism to the hydrocarbon pool, involving aldol condensations. The very short diffusion paths from the single-unit-cell thick nanosheets allows for diffusion of C_9 aromatics out of the pores before they can be converted to lighter aromatics or olefins. Al-MFI-ns shows no indication of irreversible deactivation, fully recovering original catalyst activity after regeneration, and retaining similar deactivation rates and selectivity as the fresh catalyst. Al-FMI-ns improves results for production of aromatics from light oxygenates at mild conditions, a key reaction for bio-oil upgrading.

Acknowledgements

This research was supported with funds from the Small Business Innovation Research (SBIR) program at the Department of Energy under contract 97329S11-11.

References

[1] M. Moliner, Y. Roman-Leshkov, M.E. Davis, Tin-containing zeolites are highly active catalysts for the isomerization of glucose in water, Proc. Natl. Acad. Sci. U. S. A., 107 (2010) 6164-6168.
[2] Y. Román-Leshkov, M.E. Davis, Activation of carbonyl-containing molecules with solid Lewis acids in aqueous media, ACS Catal., 1 (2011) 1566-1580.
[3] Y. Román‐Leshkov, M. Moliner, J.A. Labinger, M.E. Davis, Mechanism of glucose isomerization using a solid Lewis acid catalyst in water, Angew. Chem. Int. Ed., 49 (2010) 8954-8957.
[4] J.D. Lewis, S. Van de Vyver, A.J. Crisci, W.R. Gunther, V.K. Michaelis, R.G. Griffin, Y. Román‐Leshkov, A Continuous Flow Strategy for the Coupled Transfer Hydrogenation and Etherification of 5‐(Hydroxymethyl) furfural using Lewis Acid Zeolites, ChemSusChem, 7 (2014) 2255-2265.
[5] H.Y. Luo, D. Consoli, W.R. Gunther, Y. Román-Leshkov, Investigation of the reaction kinetics of isolated Lewis acid sites in Beta zeolites for the Meerwein-Ponndorf-Verley reduction of methyl levulinate to γ-valerolactone, J. Catal., (2014).
[6] G.W. Huber, S. Iborra, A. Corma, Synthesis of transportation fuels from biomass: chemistry, catalysts, and engineering, Chem. Rev., 106 (2006) 4044-4098.
[7] T. Prasomsri, T. Nimmanwudipong, Y. Román-Leshkov, Effective hydrodeoxygenation of biomass-derived oxygenates into unsaturated hydrocarbons by MoO 3 using low H 2 pressures, Energy Environ. Sci., 6 (2013) 1732-1738.
[8] T. Prasomsri, M. Shetty, K. Murugappan, Y. Roman, Insights into the catalytic activity and surface modification of MoO3 during the hydrodeoxygenation of lignin-derived model compounds into aromatic hydrocarbons under low hydrogen pressure, Energy Environ. Sci., (2014).
[9] S. Czernik, A. Bridgwater, Overview of applications of biomass fast pyrolysis oil, Energy & Fuels, 18 (2004) 590-598.
[10] A.J. Crisci, H. Dou, T. Prasomsri, Y. Román-Leshkov, Cascade Reactions for the Continuous and Selective Production of Isobutene from Bioderived Acetic Acid Over Zinc-Zirconia Catalysts, ACS Catal., (2014) 4196-4200.
[11] F.J. Keil, Methanol-to-hydrocarbons: process technology, Microporous Mesoporous Mater., 29 (1999) 49-66.
[12] M. Bjørgen, F. Joensen, M. Spangsberg Holm, U. Olsbye, K.-P. Lillerud, S. Svelle, Methanol to gasoline over zeolite H-ZSM-5: Improved catalyst performance by treatment with NaOH, Appl. Catal., A, 345 (2008) 43-50.
[13] J.F. Haw, W. Song, D.M. Marcus, J.B. Nicholas, The mechanism of methanol to hydrocarbon catalysis, Acc. Chem. Res., 36 (2003) 317-326.
[14] Y. Bhawe, M. Moliner-Marin, J.D. Lunn, Y. Liu, A. Malek, M. Davis, Effect of Cage Size on the Selective Conversion of Methanol to Light Olefins, ACS Catal., 2 (2012) 2490-2495.
[15] G. Busca, Acid catalysts in industrial hydrocarbon chemistry, Chem. Rev., 107 (2007) 5366-5410.
[16] H.Y. Luo, L. Bui, W.R. Gunther, E. Min, Y. Román-Leshkov, Synthesis and Catalytic Activity of Sn-MFI Nanosheets for the Baeyer–Villiger Oxidation of Cyclic Ketones, ACS Catal., 2 (2012) 2695-2699.
[17] A. Corma, From microporous to mesoporous molecular sieve materials and their use in catalysis, Chem. Rev., 97 (1997) 2373-2420.
[18] S. Mitchell, A. Bonilla, J. Pérez-Ramírez, Preparation of organic-functionalized mesoporous ZSM-5 zeolites by consecutive desilication and silanization, Mater. Chem. Phys., 127 (2011) 278-284.
[19] H.K. Beyer, Dealumination techniques for zeolites, in: Post-Synthesis Modification I, Springer, 2002, pp. 203-255.
[20] A. Corma, V. Fornés, J. Guil, S. Pergher, T.L. Maesen, J. Buglass, Preparation, characterisation and catalytic activity of ITQ-2, a delaminated zeolite, Microporous Mesoporous Mater., 38 (2000) 301-309.
[21] A. Corma, U. Diaz, V. Fornés, J. Guil, J. Martınez-Triguero, E. Creyghton, Characterization and catalytic activity of MCM-22 and MCM-56 compared with ITQ-2, J. Catal., 191 (2000) 218-224.

[22] S. Maheshwari, E. Jordan, S. Kumar, F.S. Bates, R.L. Penn, D.F. Shantz, M. Tsapatsis, Layer structure preservation during swelling, pillaring, and exfoliation of a zeolite precursor, J. Am. Chem. Soc., 130 (2008) 1507-1516.
[23] W. Fan, M.A. Snyder, S. Kumar, P.S. Lee, W.C. Yoo, A.V. McCormick, R. Lee Penn, A. Stein, M. Tsapatsis, Hierarchical nanofabrication of microporous crystals with ordered mesoporosity, Nat. Mater., 7 (2008) 984-991.
[24] M. Choi, K. Na, J. Kim, Y. Sakamoto, O. Terasaki, R. Ryoo, Stable single-unit-cell nanosheets of zeolite MFI as active and long-lived catalysts, Nature, 461 (2009) 246-249.
[25] K. Na, C. Jo, J. Kim, K. Cho, J. Jung, Y. Seo, R.J. Messinger, B.F. Chmelka, R. Ryoo, Directing zeolite structures into hierarchically nanoporous architectures, Science, 333 (2011) 328-332.
[26] J. Jung, C. Jo, K. Cho, R. Ryoo, Zeolite nanosheet of a single-pore thickness generated by a zeolite-structure-directing surfactant, J. Mater. Chem., 22 (2012) 4637.
[27] T.Q. Hoang, X. Zhu, L.L. Lobban, D.E. Resasco, R.G. Mallinson, Effects of HZSM-5 crystallite size on stability and alkyl-aromatics product distribution from conversion of propanal, Catal. Commun., 11 (2010) 977-981.
[28] X. Zhu, L.L. Lobban, R.G. Mallinson, D.E. Resasco, Tailoring the mesopore structure of HZSM-5 to control product distribution in the conversion of propanal, J. Catal., 271 (2010) 88-98.
[29] M. Milina, S. Mitchell, P. Crivelli, D. Cooke, J. Pérez-Ramírez, Mesopore quality determines the lifetime of hierarchically structured zeolite catalysts, Nat. Commun., (2014).
[30] L. Bui, H. Luo, W.R. Gunther, Y. Roman-Leshkov, Domino reaction catalyzed by zeolites with Bronsted and Lewis acid sites for the production of gamma-valerolactone from furfural, Angew. Chem. Int. Ed. Engl., 52 (2013) 8022-8025.
[31] J. Schlenker, B. Peterson, Computed X-ray powder diffraction patterns for ultrasmall zeolite crystals, J. Appl. Crystallogr., 29 (1996) 178-185.
[32] J. Boshoff, UDSKIP, http://www.che.udel.edu/research_groups/nanomodeling/resources.html, University of Delaware (2012).
[33] H. Van Koningsveld, J. Jansen, H. Van Bekkum, The monoclinic framework structure of zeolite H-ZSM-5. Comparison with the orthorhombic framework of as-synthesized ZSM-5, Zeolites, 10 (1990) 235-242.
[34] D. Bhattacharya, S. Sivasanker, A comparison of aromatization activities of the medium pore zeolites, ZSM-5, ZSM-22, and EU-1, J. Catal., 153 (1995) 353-355.
[35] T.Q. Hoang, X. Zhu, T. Sooknoi, D.E. Resasco, R.G. Mallinson, A comparison of the reactivities of propanal and propylene on HZSM-5, J. Catal., 271 (2010) 201-208.

Tables (1 total)

Table 1. Catalyst characterization.

Catalyst	Composition [a] Si/Al	Micropore volume [b] (cm^3g^{-1})	Total pore volume [c] (cm^3g^{-1})	External surface area [d] (m^2g^{-1})	Fraction tetrahedral Al [e]
Al-MFI-ns	26	0.142	0.552	357	0.438
Al-MFI-b	15	0.158	0.255	n.d.	0.862

[a] Si/Al ratio measured by ICP atomic emission spectroscopy.

[b] Micropore volume calculated from nitrogen adsorption isotherm at P/Po = 0.01.

[c] Total pore volume calculated from nitrogen adsorption isotherm at P/Po = 0.95.

[d] Surface area is the external surface area calculated from the t-plot method with nitrogen adsorption isotherm.

[e] Quantification of tetrahedrally coordinated Al sites by ^{27}Al solid state MAS NMR.

Figures (5 total)

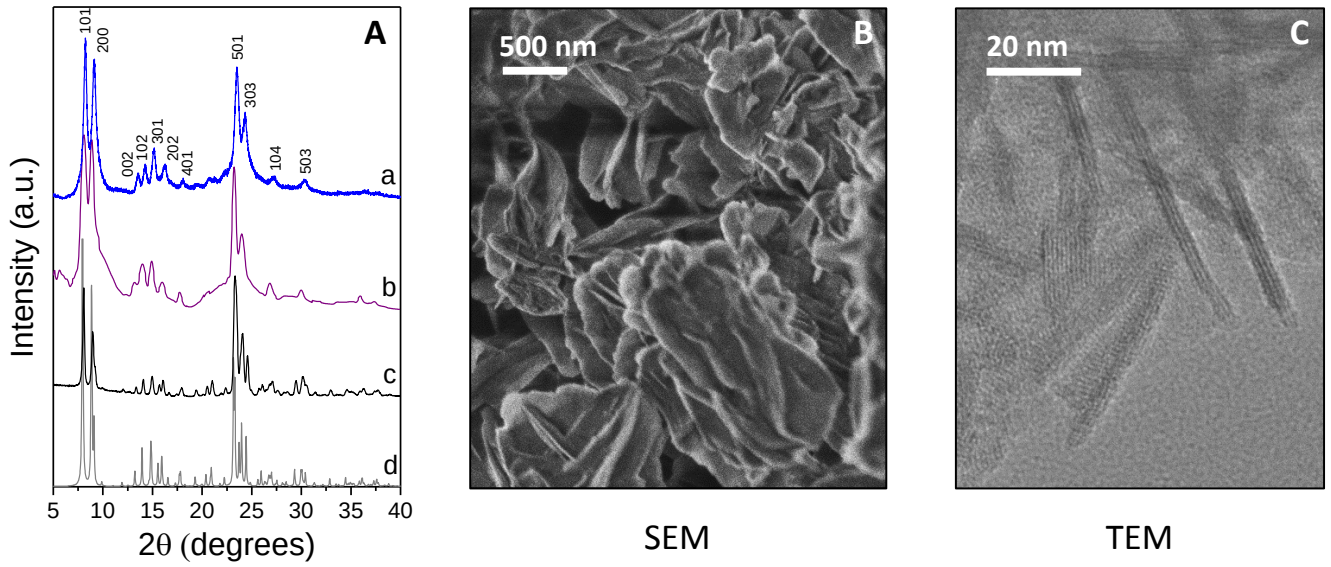

Figure 1. Characterization data of Al-MFI-ns catalysts calcined at 823 K. (A) PXRD patterns of (a) Al-MFI-ns, (b) simulated MFI nanosheets, (c) Al-MFI, and (d) simulated MFI bulk; (B) SEM image of Al-MFI-ns; (C) TEM image of Al-MFI-ns.

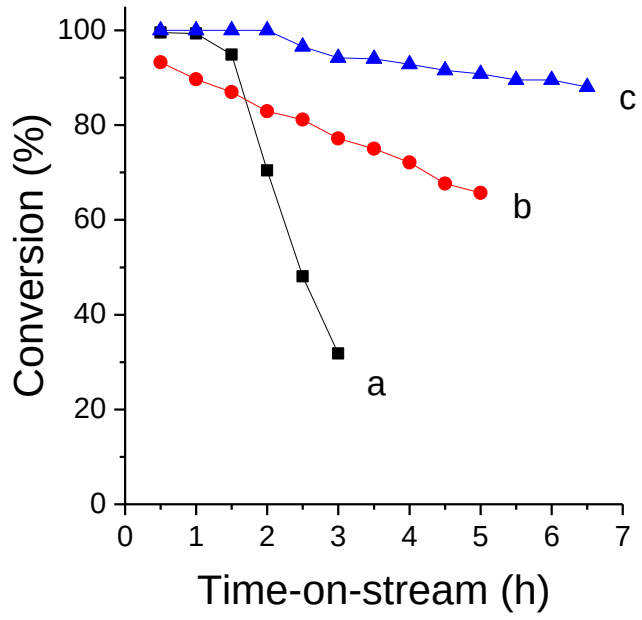

Figure 2. Conversion (mole %) of propanal over Al-containing catalysts: (a) Al-MFI, SV = 75 h^{-1}; (b) Al-MFI-ns, SV = 100 h^{-1}; (c) Al-MFI-ns, SV = 50 h^{-1}. Reaction conditions: 673 K, propanal feed rates 0.2 ml h^{-1}, He carrier gas flow 70 $mlmin^{-1}$, atmospheric pressure.

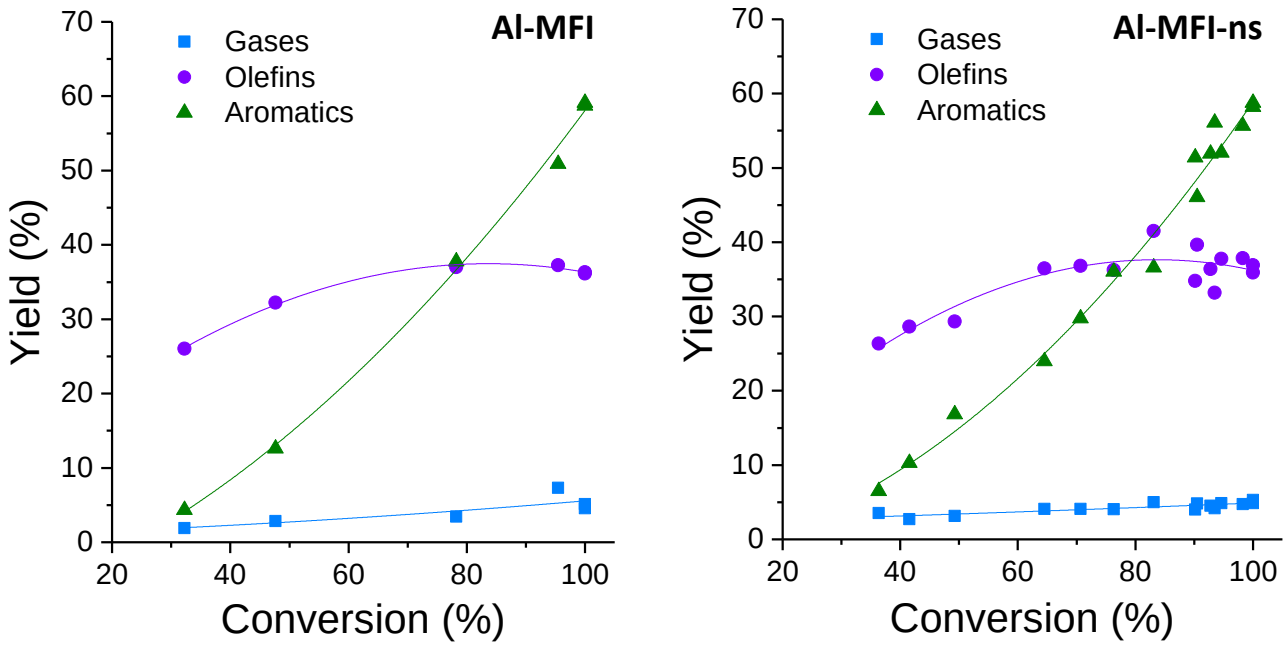

Figure 3. Product group yields as a function of conversion for propanal to hydrocarbons over Al-containing catalysts: Al-MFI (left), Al-MFI-ns (right). Reaction conditions: 673 K, SV = 50-100 h^{-1}, propanal feed rates 0.2 ml h^{-1}, He carrier gas flow 70 $mlmin^{-1}$, atmospheric pressure.

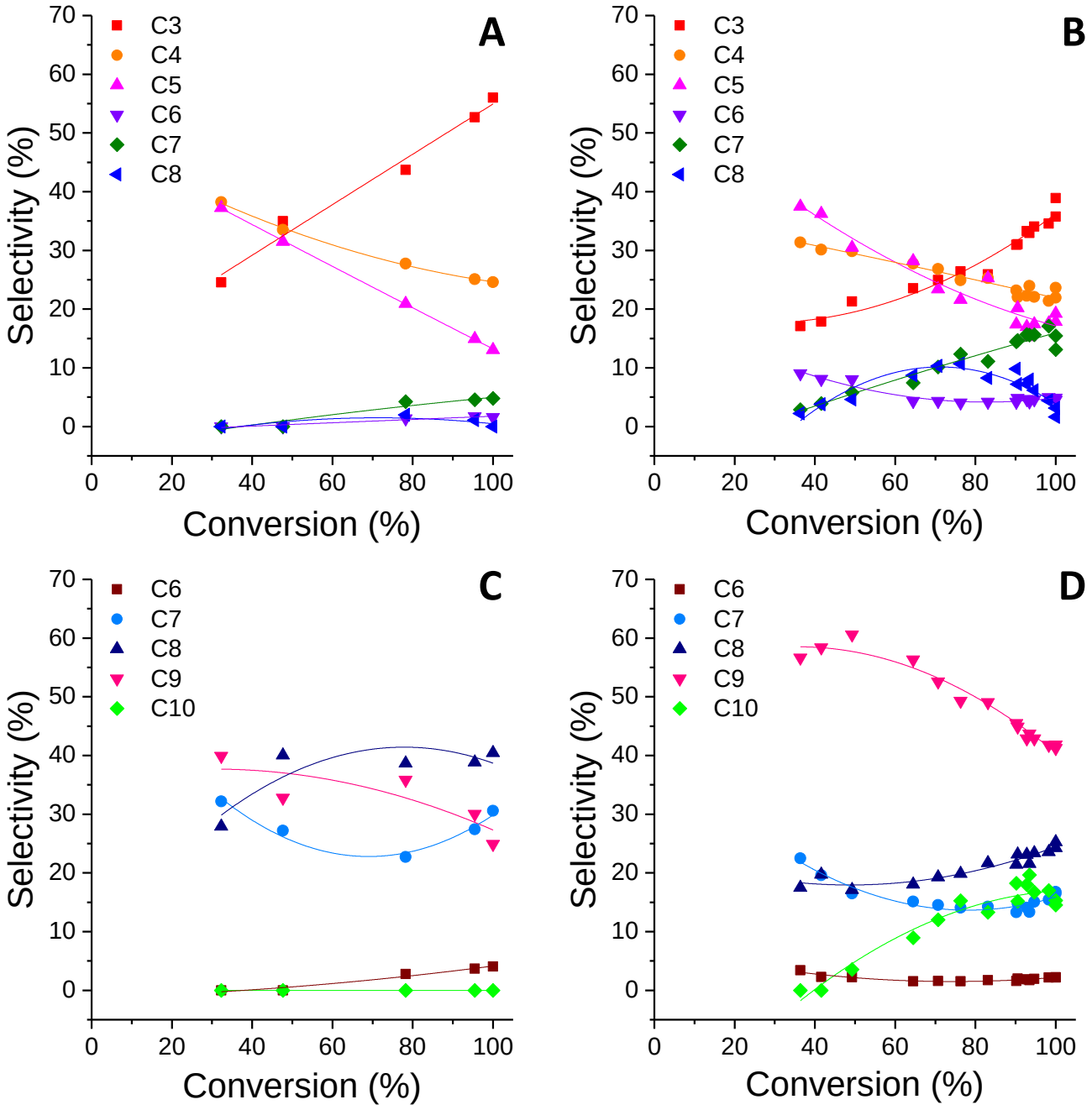

Figure 4. Olefins and aromatics product distribution as a function of conversion for propanal to hydrocarbons over Al-containing catalysts. (A) Al-MFI olefins selectivity, (B) Al-MFI-ns olefins selectivity, (C) Al-MFI aromatics selectivity, (D) Al-MFI-ns aromatics selectivity. Reaction conditions: 673 K, SV = 50-100 h^{-1}, propanal feed rates 0.2 ml h^{-1}, He carrier gas flow 70 $mlmin^{-1}$, atmospheric pressure.

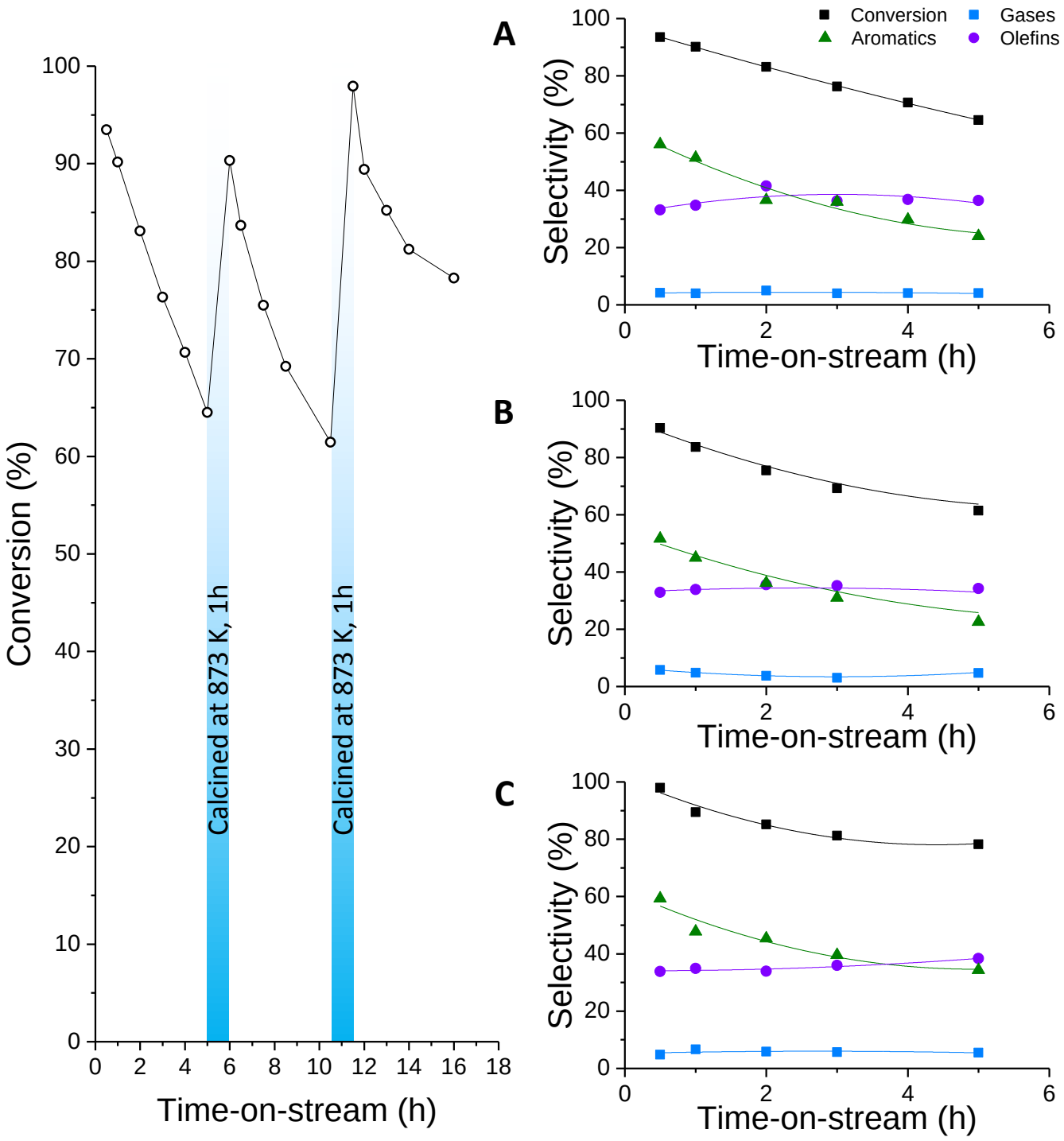

Figure 5. Conversion (mole %) of propanal over Al-MFI-ns with two 1 hr, 873 K calcinations at 5 h and 10.5 h (left). Product group yields as a function of time-on-stream for (A) fresh Al-MFI-ns, (B) once regenerated Al-MFI-ns, and (C) twice regenerated Al-MFI-ns. Reaction conditions: 673 K, SV = 100 h^{-1}, propanal feed rates 0.2 ml h^{-1}, He carrier gas flow 70 $mlmin^{-1}$, atmospheric pressure.